

From Fresh to Salty: How Ions Modulate Solvent-Mediated Interactions between Grafted Silica Nanoparticles in Water

Yuvraj Singh,¹ Chandan K. Choudhury,² and Rakesh S. Singh³

¹⁾Department of Physics, Indian Institute of Science Education and Research (IISER) Tirupati, Tirupati, Andhra Pradesh, 517619, India

²⁾Prescience Insilico Pvt. Ltd. Bengaluru, Karnataka, 530068, India

³⁾Department of Chemistry, Indian Institute of Science Education and Research (IISER) Tirupati, Tirupati, Andhra Pradesh, 517619, India^{a)}

Nanoparticles (NPs) are fundamental building blocks for engineering functional soft materials, where precise control over the solvent-mediated inter-particle effective interaction (U_{eff}) is essential for tailoring bulk structure and properties. These solvent-mediated interactions are strongly influenced by NP's surface chemistry, solvent properties, and thermodynamic conditions such as temperature (T) and pressure (P). However, despite considerable progress, a general predictive framework for tuning U_{eff} and guiding self-assembly remains lacking. In this work, using all-atom molecular dynamics simulations, we investigated the alteration of U_{eff} between silica nanoparticles (Si-NPs) functionalized with polyethylene (PE) and polyethylene glycol (PEG) by salt (sodium chloride) across a range of thermodynamic conditions. At ambient thermodynamic conditions, bare (not functionalized) Si-NPs exhibit minimal variation in U_{eff} even at high salt concentrations (up to 5 molal). In contrast, PE-grafted Si-NPs display strong salt-induced attractions, while PEG-grafted Si-NPs show an intermediate, more gradual response. To assess the transferability of these salt-induced effects on effective interactions, we further examined the effects of salt on U_{eff} under different (T, P) conditions. Our results indicate that the salt-induced modulation of U_{eff} between both bare and grafted Si-NPs is largely invariant across the explored (T, P) conditions. Molecular-level analysis reveals that salt promotes solvent depletion within the interparticle cavity for both hydrophobic PE and hydrophilic PEG grafts, with the strongest effect observed in the PE case. In general, this study highlights the coupled roles of surface chemistry, ion-polymer interactions, and solvent structuring in the regulation of U_{eff} , and provides important insights into the predictable control of interparticle interactions for soft material engineering.

I. INTRODUCTION

Nanoparticle (NP) self-assembly has emerged as a promising approach in materials science that allows bottom-up fabrication of complex materials with tailored properties^{1–5}. This methodology is central to a wide range of applications such as plasmonics^{2,6}, photovoltaics⁷, chemical and biological sensing^{8,9}, and drug delivery^{10,11}. In these systems, NPs act as fundamental building blocks where controlling their self-assembly pathways is essential to achieve targeted structural and functional outcomes. There is a growing interest in developing inverse design methods with the aim of achieving specific interaction potentials that guide the self-assembly process to the target structure. Self-assembly pathways can be systematically modulated by tuning interparticle interactions by altering intrinsic NP characteristics such as size, shape, and surface chemistry or by the surrounding solvent environment^{12–16}. Such tunability of local interparticle interactions is central to rational design of self-assembled materials^{17–20}.

Computer simulations play a crucial role in this effort by providing detailed molecular-level insights into how nanoscale building blocks (such as NPs or colloids) dispersed in a solvent interact and organize. In many systems, the solvent-mediated effective interaction (U_{eff})

between NPs is not solely determined by their intrinsic properties (such as size, shape, and surface chemistry) but is strongly influenced by the surrounding solvent^{21–25}. By tuning the solvent-mediated interactions — either through NP's surface modifications or by altering solvent properties — one can effectively control self-assembly pathways and engineer structures with tailored properties. The surface characteristics of NPs can be modulated by adjusting surface polarity, for example via polymer or DNA grafting^{26–31}, whereas the solvent properties can be tailored by introducing additives such as salts^{32–35} or alcohols^{36–38}. In the case of grafted NPs, the interplay between the solvent and the grafted polymers, as well as, solvent-NP interactions play a crucial role. For example, favorable solvent-polymer interactions typically lead to extended polymer conformations, while unfavorable interactions can induce polymer collapse or adsorption onto the NP surface^{39–41} resulting in a change in inter-NP effective interactions. These effects are not only substantial but also highly complex and depend on the system under consideration. Furthermore, thermodynamic conditions such as pressure (P) and temperature (T) can significantly influence the behavior of both solvent and polymer, thereby altering U_{eff} between NPs^{42–45}. Variations in temperature can change the solvent's behavior, affecting whether it promotes polymer swelling or collapse^{46–49}. Similarly, pressure can influence molecular packing and solvent density, which in turn modifies solvent properties and polymer

^{a)}Electronic mail: rssingh@iisertirupati.ac.in

conformations^{50–53}. These changes directly impact how NPs interact and aggregate in the medium, and therefore, understanding these effects requires elaborate computational efforts to decipher the interplay between solvent properties, NP's surface characteristics and effective inter-particle interactions.

Recently, considerable effort has been devoted to understanding how the free energy landscape (FEL) governs self-assembly and phase transition pathways^{54–60}. However, the role of effective pair interactions between constituent particles in shaping this landscape — particularly in the context of competing multiple phases — remains less explored. Recent simulation studies have shown that careful tuning of interparticle interactions can lead to a wide range of complex and hierarchical structures^{61–67} which are local minima in the FEL. For example, Truskett and coworkers⁶⁸ introduced a simulation method to adjust pair interactions, promoting the formation of specific two-dimensional lattices. This approach was later extended to three-dimensional structures using a relative entropy optimization framework⁶⁹. Similarly, Yu and Guo³¹ demonstrated that the self-assembly of polymer-grafted nanocrystals is governed by a competition between the packing entropy of the grafted polymers and the directional entropy of the core shape, enabling programmable transitions between face-centered cubic (FCC), body-centered cubic (BCC), and anisotropic superlattices.

There is a growing experimental interest in understanding how NP surface functionalization influences their assembly into ordered structures. For instance, Rogers et al.⁷⁰ demonstrated that DNA-grafted colloids can be programmed to form well-defined crystal lattices through sequence-specific interactions. Akcora et al.⁷¹ showed that polymer-grafted NPs can self-assemble into anisotropic superlattices by tuning polymer chain length and grafting density. In another example, Wang et al.⁷² reported that replacing a gold core with TiO₂ in polystyrene-grafted NPs leads to spontaneous clustering driven by enhanced interparticle attractions. To gain molecular-level insight into how surface functionalization modulates interparticle interactions and, in turn, self-assembly pathways, we recently performed simulations to examine the effect of short polymer grafts on the effective interaction U_{eff} between silica NPs (Si-NPs) dispersed in water¹⁴. Using polymers spanning hydrophobic to hydrophilic character — polyethylene (PE), polyethylene glycol (PEG), and polymethyl methacrylate (PMMA) — we found that both the strength and range of U_{eff} are highly sensitive to polymer chemistry and surface grafting density. These findings underscore the central role of surface functionalization in reliably tuning interparticle forces. Despite these advances, the influence of external additives (such as salts) on solvent-mediated NP interactions remains comparatively underexplored, particularly the molecular mechanisms by which such additives modify U_{eff} .

In the present study, we employed all-atom molecu-

lar dynamics (MD) simulations to systematically investigate the influence of sodium chloride (NaCl) salt under different (T, P) conditions on U_{eff} between bare (or, ungrafted) and grafted Si-NPs. Our results show that salt addition significantly alters the (effective) interaction strength, with the extent of this alteration depending on nature of surface functionalization (*i.e.*, hydrophilic vs hydrophobic grafting polymers). The salt-induced effects are more pronounced for hydrophobic PE-grafted Si-NPs. We further investigated the transferability of these salt-induced effects by examining the effects of salt on U_{eff} under different (T, P) conditions and surface functionalizations. To elucidate the underlying mechanisms, we also analyzed the roles of polymer-solvent interaction, ion affinity, and local solvent structuring in governing the observed changes in U_{eff} . Overall, this study highlights the coupled roles of surface chemistry, ion-surface (including grafted polymer) interactions, and solvent in governing U_{eff} , offering key insights for the rational and predictable tuning of interparticle interactions.

II. COMPUTATIONAL METHOD DETAILS

A. Model and MD simulation details

All-atom MD simulations were performed using GROMACS⁷³ (version 2021.5), coupled with PLUMED⁷⁴ (version 2.8.1). We first modeled bare Si-NP of diameter of 2 nm using CHARMM-GUI⁷⁵ and two polymer types, PE and PEG, each comprising five repeating units, were grafted onto the bare Si-NP surface to model the grafted Si-NPs. A total of 22 polymer chains were randomly attached on each particle, that is, the surface grafting density of 1.75 chains/nm². The complete modeling protocol and force field parameters are described in our previous work¹⁴. Two such NPs were placed in a cubic simulation box of 12 nm side length. This box was then solvated with TIP3P⁷⁶ water containing NaCl at concentrations of 2 molal (m) and 5 m (*i.e.*, 2 and 5 moles of salt per kg of water). Force field parameters for NaCl compatible with TIP3P were adopted from Ref. 77 that is validated against experimental salt solubility. All simulations were conducted under isothermal-isobaric (*NPT*) conditions at temperatures 300 K and 350 K, and at pressures of 1 bar and 1000 bar. Temperature was controlled using the Nosé–Hoover thermostat⁷⁸ with a relaxation time of 0.4 ps, and pressure was maintained using the Parrinello–Rahman barostat⁷⁹ with a relaxation time of 2 ps. A cutoff of 1.2 nm was applied for both van der Waals and short-range Coulomb interactions. Long-range electrostatics were treated using the particle mesh Ewald (PME) method⁸⁰. The rigid body constraints were implemented using the linear constraint solver (LINCS) algorithm⁸¹. Periodic boundary conditions were applied in all three spatial directions. The equations of motion were integrated using the Verlet algorithm with 2 fs timestep.

B. Potential of mean force (PMF) computation

The U_{eff} between NPs in water is estimated by computing the potential of mean force (PMF) as a function of the center-of-mass distance (r_{com}) between Si-NPs using the umbrella sampling method. The reaction coordinate was divided into 35 overlapping windows, spaced by 0.12 nm. A harmonic bias potential with a force constant of 1500 kJ/mol nm² was applied to each window to ensure adequate histogram overlap. For configurations with $r_{\text{com}} < 4$ nm, the systems were equilibrated for at least 200 ns, and for larger separations, equilibration times ranged from 100 – 150 ns depending on the thermodynamic condition and the nature of the grafting polymers. The initial 50% of the sampling data from each window were discarded and the remaining data were divided into five equal segments. The weighted histogram analysis method (WHAM) was applied to each segment to construct five independent PMF profiles, which were then used to assess convergence and estimate statistical errors. The final PMF profile used for analysis corresponds to the average of these five profiles. We also examined the effects of system size and equilibration time on U_{eff} by reducing the system size (number of water molecules) from $N = 50000$ to $N = 32000$ molecules (corresponding to average box lengths of approximately 12 nm and 10 nm, respectively, under near-ambient thermodynamic conditions) and extending the system equilibration time to 400 ns. The results exhibited the same qualitative trend, with U_{eff} changing approximately by maximum 10% near the contact separation for the PE-grafted case.

III. RESULTS AND DISCUSSION

A. Salt-induced modulation of solvent-mediated effective inter-Si-NP interaction

The solvent-mediated effective interaction U_{eff} between NPs — characterized by the PMF — describes the free energy profile as a function of the center-of-mass distance between two Si-NPs. We first computed U_{eff} to investigate how variations in salt concentration influence the interactions between Si-NPs in aqueous NaCl solution. Figure 1 presents the U_{eff} between two Si-NPs as a function of r_{com} under different salt concentrations for bare, PE-grafted, and PEG-grafted systems at 300 K and 1 bar. For the bare Si-NP case (Fig. 1a), U_{eff} exhibits a shallow minimum near $r_{\text{com}} \approx 2.1$ nm. The depth of this minimum (a measure of the strength of interaction) increases slightly from approximately –2.5 kJ/mol in pure water to –5.0 kJ/mol as the salt concentration increases to 5 m. This modest change suggests that the interaction between bare Si-NPs is only weakly sensitive to the presence of the NaCl salt. However, in contrast, the PE-grafted system (Fig. 1b) shows a much stronger response to the change in salt concentration. At 2 m NaCl concen-

tration, the depth of U_{eff} increases significantly to nearly –127 kJ/mol, compared to approximately –82 kJ/mol in salt-free solvent (pure water). Due to this substantial increase in attraction observed at the salt concentration 2 m, no further simulations were performed at higher salt concentrations for this (PE-grafted) system. For PEG-grafted Si-NP system (Fig. 1c), the change in U_{eff} lies in between the bare and PE-grafted cases. The depth of U_{eff} increases from approximately –2.5 kJ/mol in a salt-free solvent to approximately –25 kJ/mol at a salt concentration of 5 m. In addition, the repulsive core shifts towards a smaller diameter r_{com} with increasing salt concentration, suggesting a salt-dependent conformation change in grafted PEG polymers, resulting in a smaller effective diameter of the (grafted) Si-NP.

B. Is the salt-induced modulation of U_{eff} transferable across (T, P) conditions?

Temperature and pressure are known to significantly influence effective interactions between nanoscale particles^{42,82–84} and surfaces^{85–90}. It is therefore important to examine whether the salt-induced modulation of U_{eff} observed near ambient conditions remains transferable across different thermodynamic (T, P) states — that is, whether the extent of influence of salt on U_{eff} persists upon varying (T, P). To address this, we computed U_{eff} between two Si-NPs dispersed in solution under elevated (T, P) conditions. Figure 2 shows the modulation of U_{eff} by salt at $T = 350$ K and $P = 1$ bar, and at $T = 300$ K and $P = 1000$ bar for both bare, PEG- and PE-grafted Si-NPs. For bare Si-NPs, the U_{eff} profile exhibits only a modest change upon salt addition at elevated (T, P) conditions (see Figs. 2a(i) and 2a(ii)), consistent with the behavior observed under ambient conditions (Fig. 1(a)). This suggests that, in the low-salt regime, solvent-mediated interactions between bare Si-NPs are largely insensitive to variations in (T, P) within the (T, P) range probed in this work. The hydrophilic PEG-grafted Si-NPs also show a similar weak dependence on pressure (see Fig. S1 in the Supplementary Material).

In contrast, PE-grafted Si-NPs exhibit a much stronger response to salt under elevated (T, P) conditions, consistent with their behavior at ambient conditions. At $T = 350$ K and $P = 1$ bar, the depth of U_{eff} increases by approximately 42 kJ/mol upon the addition of 2 m salt (Fig. 2b(i)), comparable to the enhancement observed under ambient conditions (~ 45 kJ/mol; see Fig. 1b). At elevated pressure ($P = 1000$ bar, $T = 300$ K), we observe a slight increase of about 6 kJ/mol in the salt-induced deepening of U_{eff} compared to the ambient case (from ~ 45 kJ/mol near ambient pressure to ~ 51 kJ/mol at 1000 bar). These results indicate that the salt-induced enhancement of effective attraction is largely transferable across thermodynamic conditions; in other words, variations in (T, P) exert only a weak influence on the salt-induced modification of U_{eff} .

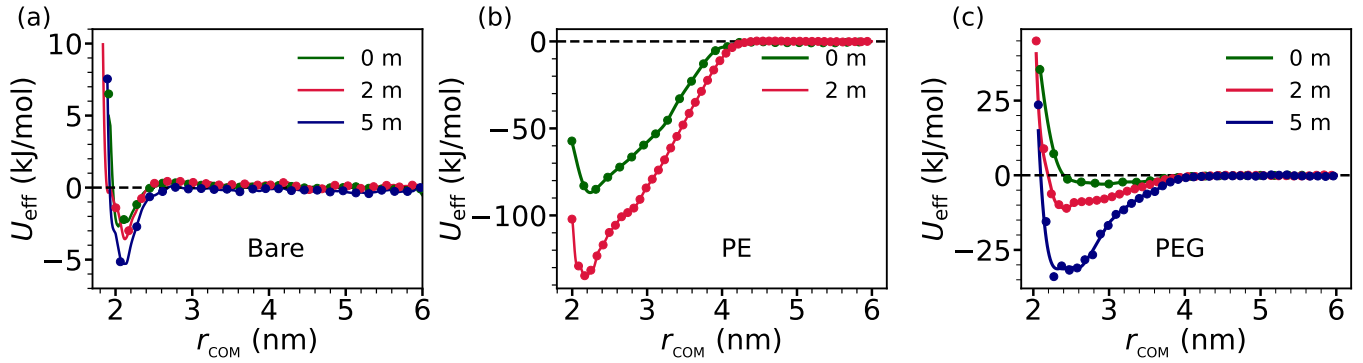


FIG. 1. The salt-dependent behavior of U_{eff} as a function of r_{com} for bare (a), PE-grafted (b), and PEG-grafted (c) systems at 1 bar and 300 K is shown. For bare Si-NP case, the absolute change in the depth of U_{eff} with increasing salt concentration is minimal with an increase of ~ 3 kJ/mol at 5 m concentration of NaCl. In contrast, the PE-grafted system exhibits a pronounced increase in the depth of U_{eff} . For the PEG-grafted case, the depth of the attractive basin increases to an intermediate extent compared to the bare and PE-grafted cases. Additionally, the hard repulsive core (a measure of the effective Si-NP diameter) shifts towards smaller r_{com} value.

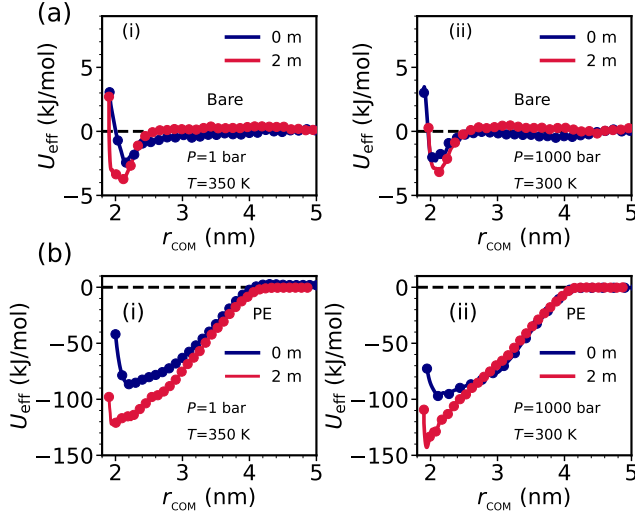


FIG. 2. The effects of salt on U_{eff} profile at elevated (with respect to ambient) pressure and temperature conditions is shown for the bare Si-NP (a) and PE-grafted Si-NP (b) systems. Here we have reported the U_{eff} profile at two thermodynamic conditions: $T = 350$ K, $P = 1$ bar and $T = 300$ K, $P = 1000$ bar; shown in (i) and (ii), respectively. For the bare Si-NP system, U_{eff} remains largely unaffected on salt addition by increase of temperature from 300 K to 350 K and pressure to 1000 bar. In contrast, the PE-grafted system shows a marked increase in the strength of attractive interaction on salt addition at elevated conditions as well.

The results presented above (Sections IIIA and IIIB) highlight the intricate coupling between the nature of the grafting polymer (*i.e.*, NP surface functionalization) and the ionic strength of the solvent in governing the effective pair interactions between nanoscale Si-NPs. These findings underscore the importance of considering both surface chemistry and solvent properties in tandem when assessing solvent-mediated forces between nanoscale build-

ing blocks.

IV. MOLECULAR ORIGIN OF THE ALTERATION OF THE EFFECTIVE INTERACTIONS BETWEEN SI-NPS

A. Density and structural behavior of solvent confined between two Si-NPs

The solvent-mediated interactions between particles strongly depend on the arrangement of solvent molecules around them and on how this arrangement evolves as the particles approach one another. To elucidate the molecular origin of the salt-dependent modulation of U_{eff} between Si-NPs (see, for example, Fig. 1), we analyzed the scaled average solvent number density ($\langle \rho_{\text{cav}}^s \rangle$), and the scaled average tetrahedral order of cavity water ($\langle q_{t/\text{cav}}^s \rangle$) of the solvent cavity formed between two Si-NPs (see Fig. S2 in the Supplementary Material). The scaled average cavity number density is defined as, $\langle \rho_{\text{cav}}^s \rangle = \langle \rho^{\text{cav}} \rangle / \langle \rho^{\text{sol}} \rangle$, where $\langle \rho^{\text{cav}} \rangle$ is the average number density of solvent (water + ions) inside the cavity and $\langle \rho^{\text{sol}} \rangle$ is the corresponding bulk solvent density under the same (T, P) conditions and salt concentration. Similarly, the scaled tetrahedral order of cavity water is defined as, $\langle q_{t/\text{cav}}^s \rangle = \langle q_t^{\text{cav}} \rangle / \langle q_t^{\text{bulk}} \rangle$, where $\langle q_t^{\text{cav}} \rangle$ is the average tetrahedral order of water molecules in the cavity and $\langle q_t^{\text{bulk}} \rangle$ is the bulk value under identical thermodynamic and salt conditions. The local tetrahedral order parameter, q_t , quantifies how closely the arrangement of a water molecule and its four nearest neighbors approaches an ideal tetrahedral geometry. For the i^{th} water molecule, it is given by⁹¹,

$$q_t(i) = 1 - \frac{3}{8} \sum_{j=1}^3 \sum_{k=j+1}^4 \left(\cos \psi_{jik} + \frac{1}{3} \right)^2, \quad (1)$$

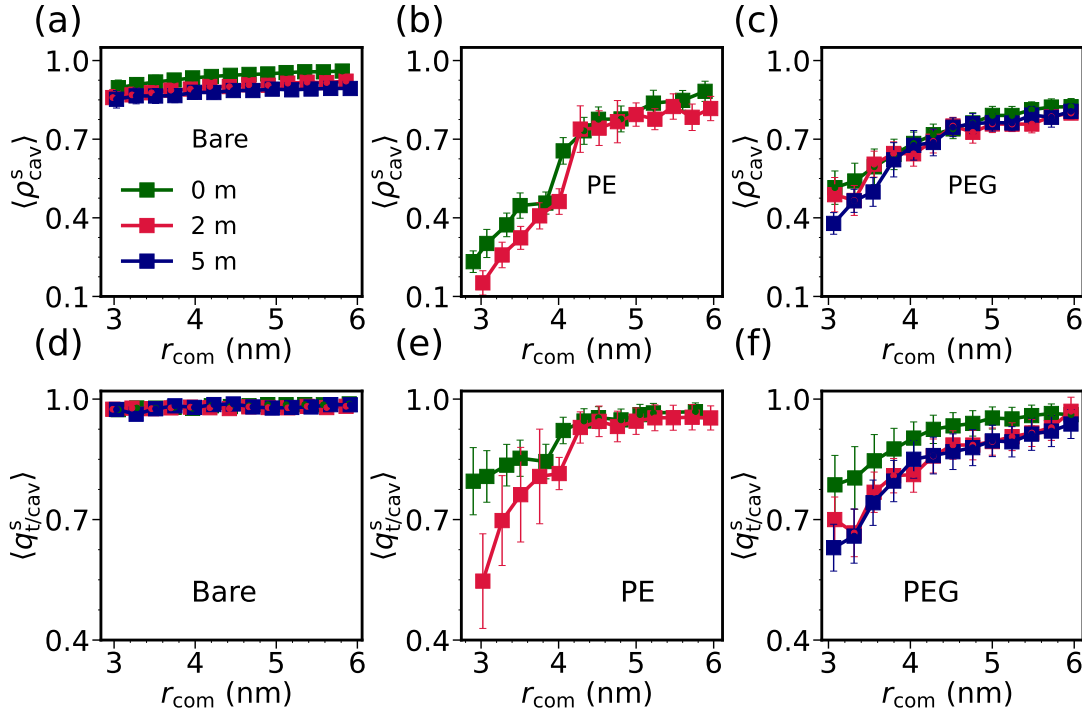


FIG. 3. Scaled average solvent number density $\langle \rho_{\text{cav}}^s \rangle$ (top, a-c) and scaled average tetrahedral order parameter $\langle q_{t/\text{cav}}^s \rangle$ (bottom, d-f) within the cavity as functions of inter-Si-NP center-of-mass separation r_{com} for bare, PE-grafted, and PEG-grafted Si-NPs at various salt concentrations. For PEG-grafted systems, $\langle \rho_{\text{cav}}^s \rangle$ decreases monotonically with increasing salt concentration, indicating enhanced solvent depletion. In the PEG-grafted case, a sharp decrease near $r_{\text{com}} = 4$ nm at 2 m salt suggests partial cavitation. The tetrahedral order parameter $\langle q_{t/\text{cav}}^s \rangle$ follows a similar trend to $\langle \rho_{\text{cav}}^s \rangle$, with water in the bare system largely retaining bulk-like structure.

where ψ_{jik} is the angle between the vectors connecting the central i^{th} water molecule to its j^{th} and k^{th} nearest neighbor. The $q_t = 1$ corresponds to perfect tetrahedral coordination, while the lower values reflect a deviation from the perfect tetrahedral structure.

In Fig. 3 we show the salt-concentration dependence of $\langle \rho_{\text{cav}}^s \rangle$ and $\langle q_{t/\text{cav}}^s \rangle$ for bare, PE-grafted, and PEG-grafted Si-NPs at 1 bar and 300 K. We find that $\langle \rho_{\text{cav}}^s \rangle$ decreases systematically with increasing salt concentration, indicating progressive solvent depletion in the cavity region. This effect is most pronounced at shorter inter-particle separations, where confinement effects are stronger. For bare Si-NPs, $\langle \rho_{\text{cav}}^s \rangle$ decreases only modestly with salt concentration (Fig. 3a), while $\langle q_{t/\text{cav}}^s \rangle$ remains nearly insensitive to salt concentration across all separations (Fig. 3d). Thus, cavity water retains a near bulk-like tetrahedral structure at low salt concentrations, regardless of cavity size. This modest solvent depletion results in only a marginal change in the depth of U_{eff} (~ 2.8 kJ/mol; Fig. 1a), corresponding to a weak enhancement in inter-particle attraction. By contrast, PE-grafted Si-NPs exhibit an abrupt decrease in $\langle \rho_{\text{cav}}^s \rangle$ near $r_{\text{com}} \approx 4.5$ nm, consistent with a partial cavitation transition — reminiscent of the cavitation or dewetting transition of water confined between two hydrophobic plates^{92,93}. A similar pronounced decrease is also

observed in $\langle q_{t/\text{cav}}^s \rangle$ at this separation, indicating a substantial disruption of the tetrahedral structure due to density loss. In our earlier study¹⁴, we attributed the strong attraction between PE-grafted Si-NPs in pure water to such cavitation-induced interactions. Interestingly, the present results show that the cavitation transition becomes increasingly pronounced as the salt concentration rises from 0 m to 2 m, leading to a strongly enhanced cavitation-induced attraction (~ 45 kJ/mol; see Fig. 1b).

The PEG-grafted system displays a more intricate response to salt concentration. Due to its hydrophilic nature, PEG tends to retain water molecules in the cavity through favorable polymer–solvent interactions. As a result, in the salt-free case, the cavity solvent density $\langle \rho_{\text{cav}}^s \rangle$ remains relatively high even at close separations compared to the hydrophobic PE-grafted case, leading to only a marginal increase in the effective attraction¹⁴. However, upon introducing salt, a sharper solvent depletion emerges near $r_{\text{com}} \approx 4$ nm (Fig. 3c), manifested in a distinct drop in both $\langle \rho_{\text{cav}}^s \rangle$ and $\langle q_{t/\text{cav}}^s \rangle$ (Figs. 3c and 3f). This depletion becomes more pronounced with increasing salt concentration and correlates directly with the enhancement of effective attraction (*i.e.*, deepening of U_{eff} near contact) between PEG-grafted Si-NPs (Fig. 1c). Also, the shift of the repulsive core toward shorter r_{com} with increasing salt concentration can be

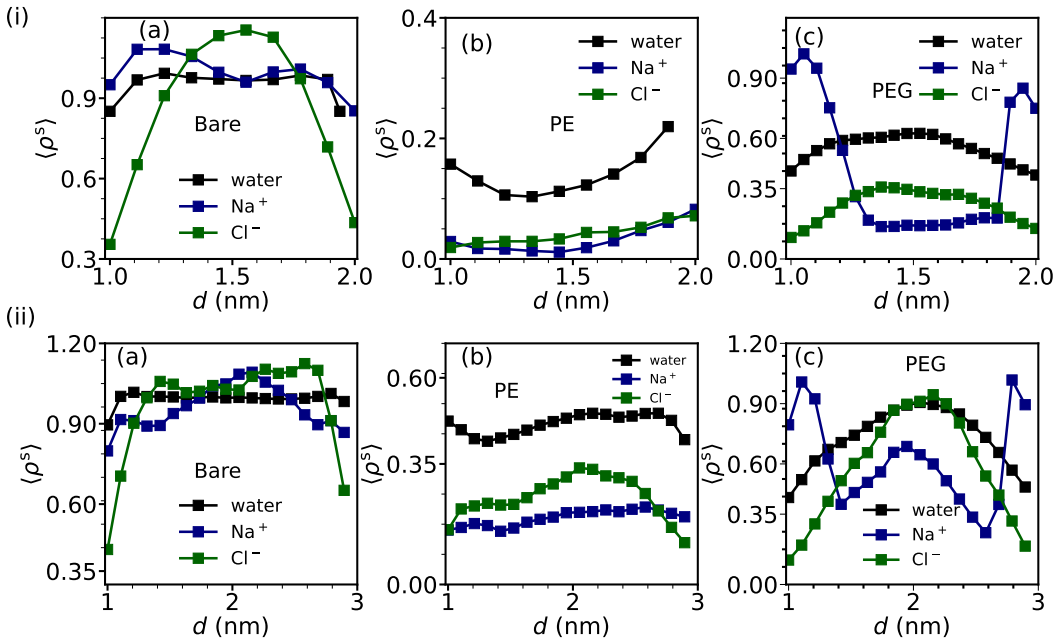


FIG. 4. Average scaled ion and water number density ($\langle \rho_s^s \rangle$) profile as a function of distance d from the centre of a Si-NP along the axis connecting the centre-of-mass of two Si-NPs (see Fig. S2 in the Supplementary Material) for $r_{\text{com}} = 3.0$ nm (i) and 4.0 nm (ii) and at 2 m salt concentration. Here, we have reported the results for bare (a), PE-grafted (b), and PEG-grafted (c) Si-NPs at temperature 300 K and pressure 1 bar. The bare and PEG-grafted Si-NP systems show enhanced Na^+ density in the vicinity of the NP — more pronounced for the PEG-grafted Si-NP indicating preferential Na^+ attraction with the PEG chains. The PE-grafted system exhibits relative lesser ion presence inside the cavity region for $r_{\text{com}} = 4.0$ nm and negligibly small for $r_{\text{com}} = 3.0$. Also, we report the absence of any preferential ion adsorption on the Si-NP surface for this case.

attributed to enhanced cavitation, which facilitates a closer approach of the PEG-grafted Si-NPs. Thus, for all systems considered (bare and grafted Si-NPs), the separation-dependent behavior of $\langle \rho_{\text{cav}}^s \rangle$ and $\langle q_{\text{t/cav}}^s \rangle$ is strongly correlated with U_{eff} , indicating that the origin of enhanced effective attraction lies in the increased propensity for solvent depletion at higher salt concentrations. Furthermore, the inter-particle separation-dependent salt density exhibits a similar trend, with Na^+ ions consistently showing higher cavity densities than Cl^- ions for hydrophilic (bare and PEG-grafted) Si-NPs, particularly at short separations (see Fig. S3 in the Supplementary Material).

B. Enhanced salt-induced cavity solvent depletion: molecular origin

To gain a deeper understanding of the molecular origin of the enhanced solvent depletion propensity from the cavity region upon salt addition for both bare and grafted Si-NPs, we examined in detail the spatial arrangement of water and ions inside the cavity. In Figs. 4(i) and 4(ii), we present the scaled (with respect to the corresponding bulk density) average water and ion density profiles along the axis connecting the centres of mass of the two Si-NPs for $r_{\text{com}} = 3.0$ nm and 4.0 nm, respectively, at 300 K, 1

bar and a salt concentration of 2 m. We find that the ion and water density profiles are strongly influenced by the nature of the grafting polymer. For bare Si-NPs, the Na^+ and water densities are enhanced in the vicinity of the Si-NP surface, whereas the Cl^- ions are repelled toward the bulk region (away from the NP surface). For the PEG-grafted Si-NPs, the Na^+ density profile displays two pronounced peaks compared to the bare Si-NP case, indicating enhanced accumulation of Na^+ ions near the PEG-grafted surfaces for both inter-Si-NP separations. This accumulation can be attributed to the preferential adsorption of Na^+ ions on the PEG chains and the Si-NP surface, arising from favorable electrostatic interactions with the electronegative oxygen atoms of PEG and Si-NPs (see Fig. S4 in the Supplementary Material). The higher Na^+ density relative to Cl^- in the cavity, discussed in the previous section (see also Fig. S3 of the Supplementary Material) can also be attributed to this preferential adsorption of Na^+ ions on PEG chains and Si-NP surface. The region near the cavity centre does not exhibit polymer-mediated preference for Na^+ , leading to lower Na^+ density there. The observed enhancement of water and Cl^- density near the cavity center, relative to the Si-NP surface, can be attributed to excluded-volume effects imposed by PEG chains near the Si-NP surface, together with the partial absence of preferential interaction sites for these species. The selective adsorption

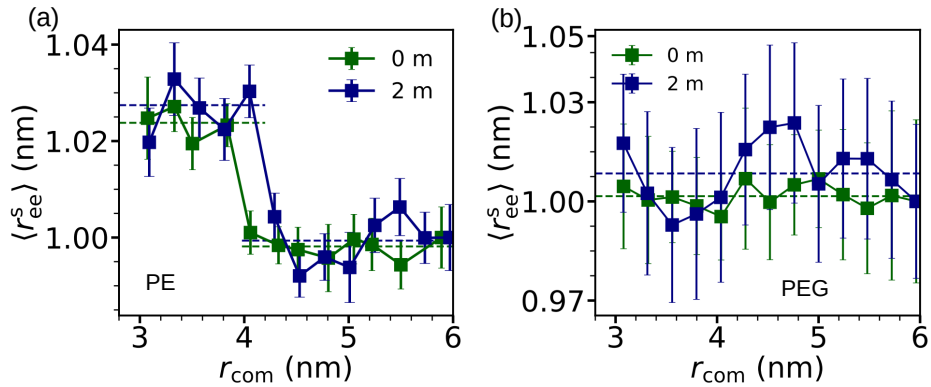


FIG. 5. Scaled mean end-to-end distance ($\langle r_{ee}^s \rangle$) of the grafting PE (a) and PEG (b) polymers as a function of inter-Si-NP center-of-mass separation (r_{com}) at temperature 300 K and 1 bar pressure. We have reported here the results for 0 m (pure water) and 2 m salt concentrations. Error bars represent standard deviations across 5 independent simulation trajectories. The dashed lines represent the average values of $\langle r_{ee}^s \rangle$ calculated over the specified ranges of r_{com} . For the PE-grafted case, the short PE chains undergo a transition to relatively elongated conformational states on the onset of the cavitation transition (see Fig. 3b). This transition gets more pronounced on adding salt to water. The PEG chains, however, show enhanced conformational fluctuations but no significant conformational change on adding salt.

of Na^+ on PEG chains screen the Si-NP surface polymer region from water by disrupting PEG-water hydrogen bonding (Na^+ ions compete with water for interactions with PEG). This process leads to hydration repulsion: the PEG polymer region becomes less hydrated, the inter-particle cavity loses water and the effective inter-particle attraction is consequently enhanced — analogous to cavitation-induced attraction between nanoscale hydrophobic surfaces.

In contrast, for PE-grafted Si-NPs, favorable salt-polymer interaction sites are absent on PE chains. As a result, salt ions interact more strongly with water molecules than with the PE chains. This effectively removes water molecules from the vicinity of the PE-grafted Si-NPs, consistent with the well-known salting-out effect^{94–100}. The salting-out process reduces the solubility of the hydrophobic PE segments, enhances solvent expulsion from the inter-particle cavity, and thus, amplifies the effective inter-particle interaction. The weak salt-polymer interaction also results in a significantly lower salt density in the cavity region at both inter-Si-NP separations (Fig. 4(i-ii)b). Overall, although the molecular mechanisms differ — hydration repulsion due to preferential ion adsorption in the PEG case versus salting-out in the PE case — salt addition promotes a common outcome: enhanced solvent depletion from the inter-particle cavity and strengthening the effective interaction between the grafted Si-NPs.

C. Manifestations of partial cavitation transition in the conformational behavior of grafting polymers

It is well established that the conformational properties of polymers are highly sensitive to both solvent characteristics and spatial confinement^{101,102}. The results re-

ported above (Sections IVC and IVD) suggest that cavity solvent properties are significantly altered when the inter-particle separation is reduced, and this alteration may lead to changes in the conformational behavior of the grafted polymers. Therefore, it is natural to probe whether signatures of solvent-induced changes in the effective Si-NP interaction are also reflected in the conformational behavior of grafted polymers at different salt concentrations. To quantify the conformational behavior of grafted polymers, we computed the scaled average end-to-end distance of the grafted PE and PEG chains ($\langle r_{ee}^s \rangle$), defined as $\langle r_{ee}^s \rangle = \langle r_{ee} \rangle / \langle r_{ee}^o \rangle$, as a function of the inter-Si-NP separation r_{com} at 0 m and 2 m salt concentration. Here, $\langle r_{ee} \rangle$ is the average end-to-end distance at a given r_{com} , and $\langle r_{ee}^o \rangle$ corresponds to the value at which the NPs are maximally separated ($r_{com} \sim 6$ nm) in the cubic simulation box with an average box length of approximately 12 nm.

The conformational behavior of the grafted polymers, characterized by $\langle r_{ee}^s \rangle$, exhibits distinct trends for PE and PEG-grafted Si-NPs (see Fig. 5). For PE-grafted Si-NPs, a sharp transition in $\langle r_{ee}^s \rangle$ is observed near $r_{com} \approx 4$ nm, which coincides with the onset inter-particle separation where the cavitation transition is observed for both salt concentrations (Fig. 3b) — consistent with our previous study in salt-free solvent¹⁴ (the cavitation transition leads to the stretching of PE chains due to the significantly reduced solvent density which allows the chains to extend more freely). This conformational transition becomes marginally more pronounced with increasing salt concentration, correlating with the salt-induced enhancement of the cavitation transition (Fig. 3b) and, in turn, the strengthening of effective inter-particle attraction (Fig. 1b). Thus, the conformational behavior of the grafted PE chains provides additional evidence for the underlying origin of the salt-induced enhance-

ment of effective (PE-grafted) Si-NP interactions. In contrast, PEG-grafted Si-NPs show no abrupt conformational change. Instead, they exhibit increased conformational fluctuations and a slight overall increase in end-to-end distance upon salt addition. This behavior suggests that a more detailed analysis of charge screening effects and polymer solubility is required to fully elucidate the underlying conformational response to solvent conditions and confinement.

V. CONCLUSIONS

In this study, we employed all-atom MD simulations to systematically investigate how the solvent-mediated effective interaction, U_{eff} , between two Si-NPs in an aqueous solution is influenced by Si-NP's surface functionalization under varying salt (NaCl) concentrations and thermodynamic conditions. Specifically, we examined the interplay between surface functionalization, solvent ionic strength, and thermodynamic conditions on the pair effective interaction. Our results reveal that salt affects the interactions of different surface-functionalized Si-NPs in distinct ways. For bare (ungrafted) Si-NPs, U_{eff} shows negligible changes with increasing salt concentration. In contrast, PE-grafted Si-NPs exhibit a pronounced increase in inter-particle attraction even at a moderate (2 m) salt concentration, which we attribute to salting-out-induced enhancement of cavitation in the inter-particle cavity. PEG-grafted systems, on the other hand, display a more gradual deepening of U_{eff} with increasing salt concentration. This behavior arises from ion-induced screening of the hydrophilic PEG chains through selective Na^+ adsorption, which weakens the water-PEG hydrogen bonds and reduces the water density in the cavity compared to salt-free water, particularly at near-contact inter-particle separations.

To assess the transferability of these salt-induced effects on effective interactions, we further examined the effects of salt on U_{eff} under different (T, P) conditions. We found that the salt-effects remain largely insensitive to variations in T and P (in the range reported in this work). To gain further insight, we analyzed the conformational response of the grafted polymers to cavity solvent depletion. For PE-grafted systems, we observed a sharp increase in chain extension near the onset of cavitation transition inter-particle separation ($r_{\text{com}} \approx 4 \text{ nm}$), which is amplified at higher salt concentrations. This coincides with the steep drop in U_{eff} at $r_{\text{com}} \approx 4 \text{ nm}$ and the enhanced inter-Si-NP attraction upon salt addition. In contrast, PEG chains exhibit enhanced conformational fluctuations and only a marginal increase in chain length with rising salt concentration.

To summarize, our results underscore the complex and cooperative mechanisms by which solvent composition, and surface chemistry govern U_{eff} between nanoscale particles dispersed in solution. Such understanding, and the ability to predictably control U_{eff} , contributes to

broader efforts in inverse materials design, enabling the programmable self-assembly of nanoscale building blocks through tailored surface functionalization and solvent engineering.

VI. ACKNOWLEDGEMENTS

R.S.S. acknowledges financial support from DST-SERB (Grant No. CRG/2023/002975). Y.S. acknowledges financial support from IISER Tirupati. The computations were performed at the IISER Tirupati computing facility and at PARAM Brahma at IISER Pune.

REFERENCES

- 1 S. C. Glotzer and M. J. Solomon, "Anisotropy of building blocks and their assembly into complex structures," *Nature materials* **6**, 557–562 (2007).
- 2 J. A. Fan, C. Wu, K. Bao, J. Bao, R. Bardhan, N. J. Halas, V. N. Manoharan, P. Nordlander, G. Shvets, and F. Capasso, "Self-assembled plasmonic nanoparticle clusters," *science* **328**, 1135–1138 (2010).
- 3 M. Grzelczak, J. Vermant, E. M. Furst, and L. M. Liz-Marzán, "Directed self-assembly of nanoparticles," *ACS nano* **4**, 3591–3605 (2010).
- 4 J. B. Edel, A. A. Kornyshev, and M. Urbakh, "Self-assembly of nanoparticle arrays for use as mirrors, sensors, and antennas," *ACS nano* **7**, 9526–9532 (2013).
- 5 Y. Zhou, R. L. Marson, G. van Anders, J. Zhu, G. Ma, P. Ercius, K. Sun, B. Yeom, S. C. Glotzer, and N. A. Kotov, "Biomimetic hierarchical assembly of helical supraparticles from chiral nanoparticles," *ACS nano* **10**, 3248–3256 (2016).
- 6 K. A. Willets and R. P. Van Duyne, "Localized surface plasmon resonance spectroscopy and sensing," *Annu. Rev. Phys. Chem.* **58**, 267–297 (2007).
- 7 M. Karg, T. A. König, M. Retsch, C. Stelling, P. M. Reichstein, T. Honold, M. Thelakkat, and A. Fery, "Colloidal self-assembly concepts for light management in photovoltaics," *Materials Today* **18**, 185–205 (2015).
- 8 K. Saha, S. S. Agasti, C. Kim, X. Li, and V. M. Rotello, "Gold nanoparticles in chemical and biological sensing," *Chemical reviews* **112**, 2739–2779 (2012).
- 9 A. Karnwal, R. S. Kumar Sachan, I. Devgon, J. Devgon, G. Pant, M. Panchpuri, A. Ahmad, M. B. Alshammari, K. Hossain, and G. Kumar, "Gold nanoparticles in nanobiotechnology: from synthesis to biosensing applications," *ACS omega* **9**, 29966–29982 (2024).
- 10 J. Yang, C. Jia, and J. Yang, "Designing nanoparticle-based drug delivery systems for precision medicine," *International journal of medical sciences* **18**, 2943 (2021).
- 11 M. J. Mitchell, M. M. Billingsley, R. M. Haley, M. E. Wechsler, N. A. Peppas, and R. Langer, "Engineering precision nanoparticles for drug delivery," *Nature reviews drug discovery* **20**, 101–124 (2021).
- 12 Q. Chen, J. Yan, J. Zhang, S. C. Bae, and S. Granick, "Janus and multiblock colloidal particles," *Langmuir* **28**, 13555–13561 (2012).
- 13 E. R. Liepold, A. Smith, B. Lin, J. De Pablo, and S. A. Rice, "Pair and many-body interactions between ligated au nanoparticles," *The Journal of chemical physics* **150** (2019).
- 14 Y. Singh, C. K. Choudhury, R. Ghosh, and R. S. Singh, "Computational investigation of the effects of polymer grafting on the effective interaction between silica nanoparticles in water," *Soft Matter* **20**, 7122–7132 (2024).

¹⁵G. Hummer, S. Garde, A. E. Garcia, M. E. Paulaitis, and L. R. Pratt, "The pressure dependence of hydrophobic interactions is consistent with the observed pressure denaturation of proteins," *Proceedings of the National Academy of Sciences* **95**, 1552–1555 (1998).

¹⁶Y. Li, M. Girard, M. Shen, J. A. Millan, and M. Olvera de la Cruz, "Strong attractions and repulsions mediated by monovalent salts," *Proceedings of the National Academy of Sciences* **114**, 11838–11843 (2017).

¹⁷Z. Lu and Y. Yin, "Colloidal nanoparticle clusters: functional materials by design," *Chemical Society Reviews* **41**, 6874–6887 (2012).

¹⁸V. Linko, H. Zhang, Nonappa, M. A. Kostiainen, and O. Ikkala, "From precision colloidal hybrid materials to advanced functional assemblies," *Accounts of Chemical Research* **55**, 1785–1795 (2022).

¹⁹A. E. Baumann, D. A. Burns, B. Liu, and V. S. Thoi, "Metal-organic framework functionalization and design strategies for advanced electrochemical energy storage devices," *Communications Chemistry* **2**, 86 (2019).

²⁰E. Bianchi, B. Capone, I. Coluzza, L. Rovigatti, and P. D. Van Oostrum, "Limiting the valence: advancements and new perspectives on patchy colloids, soft functionalized nanoparticles and biomolecules," *Physical Chemistry Chemical Physics* **19**, 19847–19868 (2017).

²¹O. Galteland, F. Bresme, and B. Hafskjold, "Solvent-mediated forces between ellipsoidal nanoparticles adsorbed at liquid–vapor interfaces," *Langmuir* **36**, 14530–14538 (2020).

²²F. Bresme, H. Lehle, and M. Oettel, "Solvent-mediated interactions between nanoparticles at fluid interfaces," *The Journal of chemical physics* **130** (2009).

²³E. Prince, P. Narayanan, M. Chekini, C. Pace-Tonna, M. G. Roberts, E. Zhulina, and E. Kumacheva, "Solvent-mediated isolation of polymer-grafted nanoparticles," *Macromolecules* **53**, 4533–4540 (2020).

²⁴D. Thirumalai, G. Reddy, and J. E. Straub, "Role of water in protein aggregation and amyloid polymorphism," *Accounts of chemical research* **45**, 83–92 (2012).

²⁵Y. Kopel and N. Giovambattista, "Comparative study of water-mediated interactions between hydrophilic and hydrophobic nanoscale surfaces," *The Journal of Physical Chemistry B* **123**, 10814–10824 (2019).

²⁶L. Peng, C. S. Wu, M. You, D. Han, Y. Chen, T. Fu, M. Ye, and W. Tan, "Engineering and applications of dna-grafted polymer materials," *Chemical science* **4**, 1928–1938 (2013).

²⁷V. Subjakova, V. Oravcová, and T. Hianik, "Polymer nanoparticles and nanomotors modified by dna/rna aptamers and antibodies in targeted therapy of cancer," *Polymers* **13**, 341 (2021).

²⁸X. Ma, X. Li, G. Luo, and J. Jiao, "Dna-functionalized gold nanoparticles: Modification, characterization, and biomedical applications," *Frontiers in chemistry* **10**, 1095488 (2022).

²⁹L. Parolini, J. Kotar, L. Di Michele, and B. M. Moghetti, "Controlling self-assembly kinetics of dna-functionalized liposomes using toehold exchange mechanism," *ACS nano* **10**, 2392–2398 (2016).

³⁰F. Sciotino, Y. Zhang, O. Gang, and S. K. Kumar, "Combinatorial-entropy-driven aggregation in dna-grafted nanoparticles," *ACS nano* **14**, 5628–5635 (2020).

³¹C. Yu and H. Guo, "Molecular dynamics simulation study on self-assembly of polymer-grafted nanocrystals: From isotropic cores to anisotropic cores," *Journal of Chemical Theory and Computation* **20**, 1625–1635 (2023).

³²A. Benavides, J. Aragones, and C. Vega, "Consensus on the solubility of nacl in water from computer simulations using the chemical potential route," *The Journal of chemical physics* **144** (2016).

³³A. Ali, T. T. B. Le, A. Striolo, and D. R. Cole, "Salt effects on the structure and dynamics of interfacial water on calcite probed by equilibrium molecular dynamics simulations," *The Journal of Physical Chemistry C* **124**, 24822–24836 (2020).

³⁴Y. Ding, A. A. Hassanali, and M. Parrinello, "Anomalous water diffusion in salt solutions," *Proceedings of the National Academy of Sciences* **111**, 3310–3315 (2014).

³⁵S. Blazquez, J. L. Abascal, J. Lagerweij, P. Habibi, P. Dey, T. J. Vlugt, O. A. Moulton, and C. Vega, "Computation of electrical conductivities of aqueous electrolyte solutions: Two surfaces, one property," *Journal of chemical theory and computation* **19**, 5380–5393 (2023).

³⁶R. Ghosh and B. Bagchi, "Temperature dependence of static and dynamic heterogeneities in a water–ethanol binary mixture and a study of enhanced, short-lived fluctuations at low concentrations," *The Journal of Physical Chemistry B* **120**, 12568–12583 (2016).

³⁷S. Y. Noskov, G. Lamoureux, and B. Roux, "Molecular dynamics study of hydration in ethanol–water mixtures using a polarizable force field," *The Journal of Physical Chemistry B* **109**, 6705–6713 (2005).

³⁸L. Zhang, Q. Wang, Y.-C. Liu, and L.-Z. Zhang, "On the mutual diffusion properties of ethanol–water mixtures," *The Journal of chemical physics* **125** (2006).

³⁹P. Linse, "Effect of solvent quality on the polymer adsorption from bulk solution onto planar surfaces," *Soft Matter* **8**, 5140–5150 (2012).

⁴⁰P. Polanowski and A. Sikorski, "Monte carlo simulations of polymer collapse in an explicit solvent of varying quality," *Polymers* **17**, 978 (2025).

⁴¹D. Mukherji, C. M. Marques, and K. Kremer, "Polymer collapse in miscible good solvents is a generic phenomenon driven by preferential adsorption," *Nature communications* **5**, 4882 (2014).

⁴²S. Salas Sanabria and L. A. Hanson, "Pressure and composition effects on a common nanoparticle ligand–solvent pair," *The Journal of Physical Chemistry B* **128**, 841–848 (2024).

⁴³H. O. Yadav, G. Shrivastav, M. Agarwal, and C. Chakravarty, "Effective interactions between nanoparticles: Creating temperature-independent solvation environments for self-assembly," *The Journal of Chemical Physics* **144** (2016).

⁴⁴T. Hatakeyama, T. Hashimoto, and H. Kanetsuna, "Compressibility of polyethylene under pressure up to 5000 kg/cm²," *Colloid and Polymer Science* **252**, 15–19 (1974).

⁴⁵P. A. A. Herrera, F. Zheng, P. Zhang, J. Reitenbach, H. Amenitsch, C. Henschel, A. Laschewsky, P. Müller-Buschbaum, A. Schulte, and C. M. Papadakis, "Effect of pressure on the micellar structure and aggregation behavior of pmma-b-pnipam diblock copolymers in a water/methanol mixture," *Soft Matter* **21**, 4681–4691 (2025).

⁴⁶S. Backes, P. Krause, W. Tabaka, M. U. Witt, D. Mukherji, K. Kremer, and R. von Klitzing, "Poly (n-isopropylacrylamide) microgels under alcoholic intoxication: When a lcst polymer shows swelling with increasing temperature," *ACS Macro Letters* **6**, 1042–1046 (2017).

⁴⁷F. Piguet, H. Ouldali, F. Discala, M.-F. Breton, J. C. Behrends, J. Pelta, and A. Oukhaled, "High temperature extends the range of size discrimination of nonionic polymers by a biological nanopore," *Scientific Reports* **6**, 38675 (2016).

⁴⁸A. B. Mrad, N. Sheibat-Othman, A. P. A. Amorim, R. L. Do Rosario, and T. F. McKenna, "Polyethylene slurries: swelling and solubility," *Macromolecular Reaction Engineering* **17**, 2300020 (2023).

⁴⁹A. Alizadeh, V. Touloupidis, and J. B. Soares, "Systematic comparison of slurry and gas-phase polymerization of ethylene: Part i thermodynamic effects," *Macromolecular Reaction Engineering* **15**, 2100006 (2021).

⁵⁰T. E. de Oliveira, P. A. Netz, D. Mukherji, and K. Kremer, "Why does high pressure destroy co-non-solvency of pnipam in aqueous methanol?" *Soft Matter* **11**, 8599–8604 (2015).

⁵¹Y. Tsujita, T. Nose, and T. Hata, "Thermodynamic properties of poly (ethylene glycol) and poly (tetrahydrofuran). i. p–v–t relations and internal pressure," *Polymer Journal* **5**, 201–207 (1973).

⁵²L. Capt and M. Kamal, "The pressure-volume-temperature behavior polyethylene melts," *International Polymer Processing* **15**, 83–94 (2000).

⁵³L. Fontana, M. Santoro, R. Bini, D. Q. Vinh, and S. Scandolo, "High-pressure vibrational properties of polyethylene," *The Journal of chemical physics* **133** (2010).

⁵⁴P. R. t. Wolde and D. Frenkel, "Enhancement of protein crystal nucleation by critical density fluctuations," *Science* **277**, 1975–1978 (1997).

⁵⁵G. Ramesh, V. Mahajan, D. Koner, and R. S. Singh, "Microscopic pathways of transition from low-density to high-density amorphous phase of water," *The Journal of Chemical Physics* **160** (2024).

⁵⁶M. Iwamatsu, "Free-energy landscape of nucleation with an intermediate metastable phase studied using capillarity approximation," *The Journal of chemical physics* **134** (2011).

⁵⁷M. Santra, R. S. Singh, and B. Bagchi, "Nucleation of a stable solid from melt in the presence of multiple metastable intermediate phases: Wetting, ostwald's step rule, and vanishing polymorphs," *The Journal of Physical Chemistry B* **117**, 13154–13163 (2013).

⁵⁸M. Santra, R. S. Singh, and B. Bagchi, "Polymorph selection during crystallization of a model colloidal fluid with a free energy landscape containing a metastable solid," *Physical Review E* **98**, 032606 (2018).

⁵⁹Y. Singh, M. Santra, and R. S. Singh, "Manifestations of the possible thermodynamic origin of supercooled water's anomalies in non-classical vapour nucleation at negative pressures," *Molecular Physics* , e2491724 (2025).

⁶⁰Y. Singh, M. Santra, and R. S. Singh, "Anomalous vapor and ice nucleation in water at negative pressures: A classical density functional theory study," *The Journal of Physical Chemistry B* **127**, 3312–3324 (2023).

⁶¹A. I. Curatolo, O. Kimchi, C. P. Goodrich, R. K. Krueger, and M. P. Brenner, "A computational toolbox for the assembly yield of complex and heterogeneous structures," *Nature Communications* **14**, 8328 (2023).

⁶²W. M. Jacobs, A. Reinhardt, and D. Frenkel, "Rational design of self-assembly pathways for complex multicomponent structures," *Proceedings of the National Academy of Sciences* **112**, 6313–6318 (2015).

⁶³M. Grunwald and P. L. Geissler, "Patterns without patches: Hierarchical self-assembly of complex structures from simple building blocks," *ACS nano* **8**, 5891–5897 (2014).

⁶⁴J. Bohlín, A. J. Turberfield, A. A. Louis, and P. Sulc, "Designing the self-assembly of arbitrary shapes using minimal complexity building blocks," *ACS nano* **17**, 5387–5398 (2023).

⁶⁵A. Jain, J. A. Bollinger, T. M. Truskett, and F. A. Escobedo, "Inverse methods for material design," *AIChE Journal* **60**, 2732–2740 (2014).

⁶⁶M. Z. Miskin, H. M. Jaeger, and T. M. Truskett, "Designing allosteric control in soft materials," *Proceedings of the National Academy of Sciences* **113**, 8384–8389 (2016).

⁶⁷J. Han, S. J. Lee, D. H. Kim, and T. M. Truskett, "Reinforcement learning for inverse design of crystalline materials," *Science Advances* **5**, eaax4495 (2019).

⁶⁸B. A. Lindquist, R. B. Jadrich, and T. M. Truskett, "Communication: Inverse design for self-assembly via on-the-fly optimization," *The Journal of Chemical Physics* **145** (2016).

⁶⁹B. A. Lindquist, R. B. Jadrich, W. D. Piñeros, and T. M. Truskett, "Inverse design of self-assembling frank-kasper phases and insights into emergent quasicrystals," *The Journal of Physical Chemistry B* **122**, 5547–5556 (2018).

⁷⁰W. B. Rogers, W. M. Shih, and V. N. Manoharan, "Using dna to program the self-assembly of colloidal nanoparticles and microparticles," *Nature Reviews Materials* **1**, 1–14 (2016).

⁷¹P. Akcora, H. Liu, S. K. Kumar, J. Moll, Y. Li, B. C. Benicewicz, L. S. Schadler, D. Acehan, A. Z. Panagiotopoulos, V. Pryamitsyn, *et al.*, "Anisotropic self-assembly of spherical polymer-grafted nanoparticles," *Nature materials* **8**, 354–359 (2009).

⁷²X. Wang, S. Bhadauriya, R. Zhang, P. Pitliya, D. Raghavan, J. Zhang, M. R. Bockstaller, J. F. Douglas, and A. Karim, "Nanoimprint directed assembly of associating polymer-grafted nanoparticles for polymer thin films with enhanced stability," *ACS Applied Polymer Materials* **1**, 3242–3252 (2019).

⁷³D. Van Der Spoel, E. Lindahl, B. Hess, G. Groenhof, A. E. Mark, and H. J. Berendsen, "Gromacs: fast, flexible, and free," *Journal of computational chemistry* **26**, 1701–1718 (2005).

⁷⁴M. Bonomi, D. Branduardi, G. Bussi, C. Camilloni, D. Provasi, P. Raiteri, D. Donadio, F. Marinelli, F. Pietrucci, R. A. Broglia, *et al.*, "Plumed: A portable plugin for free-energy calculations with molecular dynamics," *Computer Physics Communications* **180**, 1961–1972 (2009).

⁷⁵P. E. Lopes, V. Murashov, M. Tazi, E. Demchuk, and A. D. MacKerell, "Development of an empirical force field for silica: application to the quartz- water interface," *The Journal of Physical Chemistry B* **110**, 2782–2792 (2006).

⁷⁶W. L. Jorgensen, J. Chandrasekhar, J. D. Madura, R. W. Impey, and M. L. Klein, "Comparison of simple potential functions for simulating liquid water," *The Journal of chemical physics* **79**, 926–935 (1983).

⁷⁷T. Yagasaki, M. Matsumoto, and H. Tanaka, "Lennard-jones parameters determined to reproduce the solubility of nacl and kcl in spc/e, tip3p, and tip4p/2005 water," *Journal of Chemical Theory and Computation* **16**, 2460–2473 (2020).

⁷⁸S. U. I. NOSÉ, "A molecular dynamics method for simulations in the canonical ensemble," *Molecular physics* **100**, 191–198 (2002).

⁷⁹M. Parrinello and A. Rahman, "Polymorphic transitions in single crystals: A new molecular dynamics method," *Journal of Applied physics* **52**, 7182–7190 (1981).

⁸⁰U. Essmann, L. Perera, M. L. Berkowitz, T. Darden, H. Lee, and L. G. Pedersen, "A smooth particle mesh ewald method," *The Journal of chemical physics* **103**, 8577–8593 (1995).

⁸¹B. Hess, H. Bekker, H. J. Berendsen, and J. G. Fraaije, "Lincs: A linear constraint solver for molecular simulations," *Journal of computational chemistry* **18**, 1463–1472 (1997).

⁸²S. L. Fiedler, S. Izvekov, and A. Violi, "The effect of temperature on nanoparticle clustering," *Carbon* **45**, 1786–1794 (2007).

⁸³S. Ferdous, M. A. Ioannidis, and D. E. Henneke, "Effects of temperature, ph, and ionic strength on the adsorption of nanoparticles at liquid–liquid interfaces," *Journal of Nanoparticle Research* **14**, 850 (2012).

⁸⁴M. A. Schroer, F. Schulz, F. Lehmküller, J. Möller, A. J. Smith, H. Lange, T. Vossmeyer, and G. Grübel, "Tuning the interaction of nanoparticles from repulsive to attractive by pressure," *The Journal of Physical Chemistry C* **120**, 19856–19861 (2016).

⁸⁵R. Zangi and B. Berne, "Temperature dependence of dimerization and dewetting of large-scale hydrophobes: a molecular dynamics study," *The Journal of Physical Chemistry B* **112**, 8634–8644 (2008).

⁸⁶T. Ghosh, A. E. García, and S. Garde, "Molecular dynamics simulations of pressure effects on hydrophobic interactions," *J. Am. Chem. Soc.* **123**, 10997–11003 (2001).

⁸⁷M. Chen, H. Zhou, R. Zhu, and H. He, "Pressure-temperature diagram of wetting and dewetting in a hydrophobic grain boundary and the liquidlike to icelike transition of monolayer water," *Phys. Rev. B* **101**, 165432 (2020).

⁸⁸N. Giovambattista, P. J. Rossky, and P. G. Debenedetti, "Effect of pressure on the phase behavior and structure of water confined between nanoscale hydrophobic and hydrophilic plates," *Phys. Rev. E* **73**, 041604 (2006).

⁸⁹J. Engstler and N. Giovambattista, "Temperature effects on water-mediated interactions at the nanoscale," *The Journal of Physical Chemistry B* **122**, 8908–8920 (2018).

⁹⁰J. Engstler and N. Giovambattista, "Different temperature- and pressure-effects on the water-mediated interactions between hydrophobic, hydrophilic, and hydrophobic–hydrophilic nanoscale surfaces," *The Journal of Chemical Physics* **157**, 064701 (2022).

⁹¹J. R. Errington and P. G. Debenedetti, "Relationship between structural order and the anomalies of liquid water," *Nature* **409**,

318–321 (2001).

⁹²M. Kanduč, A. Schlaich, E. Schneck, and R. R. Netz, “Water-Mediated Interactions between Hydrophilic and Hydrophobic Surfaces,” *Langmuir* **32**, 8767 (2016).

⁹³S. Sharma and P. G. Debenedetti, “Evaporation rate of water in hydrophobic confinement,” *Proc. Natl. Acad. Sci.* **109**, 4365 (2012).

⁹⁴M. J. Hey, D. P. Jackson, and H. Yan, “The salting-out effect and phase separation in aqueous solutions of electrolytes and poly (ethylene glycol),” *Polymer* **46**, 2567–2572 (2005).

⁹⁵R. Sadeghi and F. Jahani, “Salting-in and salting-out of water-soluble polymers in aqueous salt solutions,” *The Journal of Physical Chemistry B* **116**, 5234–5241 (2012).

⁹⁶S. Endo, A. Pfennigsdorff, and K.-U. Goss, “Salting-out effect in aqueous nacl solutions: trends with size and polarity of solute molecules,” *Environmental Science & Technology* **46**, 1496–1503 (2012).

⁹⁷A. Kalra, N. Tugcu, S. M. Cramer, and S. Garde, “Salting-in and salting-out of hydrophobic solutes in aqueous salt solutions,” *The Journal of Physical Chemistry B* **105**, 6380–6386 (2001).

⁹⁸E. E. Bruce, P. T. Bui, M. Cao, P. S. Cremer, and N. F. Van Der Vegt, “Contact ion pairs in the bulk affect anion interactions with poly (n-isopropylacrylamide),” *The Journal of Physical Chemistry B* **125**, 680–688 (2021).

⁹⁹R. Chudoba, J. Heyda, and J. Dzubiella, “Tuning the collapse transition of weakly charged polymers by ion-specific screening and adsorption,” *Soft matter* **14**, 9631–9642 (2018).

¹⁰⁰E. Kesselman, O. Ramon, R. Berkovici, and Y. Paz, “Atriftir studies on the effect of strong salting-out salts on the phase separation scenario in aqueous solutions of poly (n-isopropylacrylamide)[pnipa],” *Polymers for Advanced Technologies* **13**, 982–991 (2002).

¹⁰¹C. Williams, F. Brochard, and H. Frisch, “Polymer collapse,” *Annual Review of Physical Chemistry* **32**, 433–451 (1981).

¹⁰²J. Kraus, P. Müller-Buschbaum, T. Kuhlmann, D. Schubert, and M. Stamm, “Confinement effects on the chain conformation in thin polymer films,” *Europhysics Letters* **49**, 210 (2000)

Supplementary Material

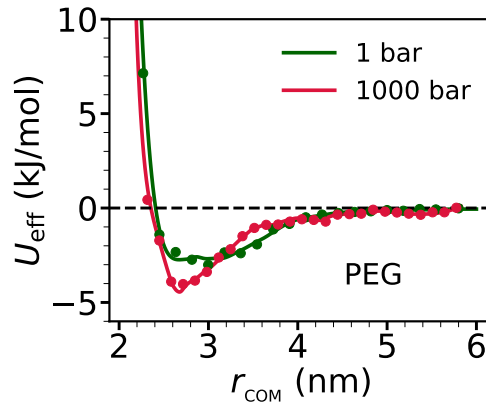


FIG. S1. The effects of pressure change on U_{eff} between two PEG-grafted Si-NPs at 300 K in a salt-free solvent is presented. Similar to the bare Si-NP case, the U_{eff} between PEG-grafted S-NPs exhibits only a weak dependence on pressure change.

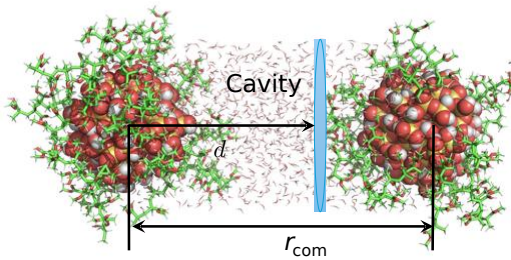


FIG. S2. Polymer-grafted Si-NPs are shown with solvent molecules occupying the interparticle cavity region. The distance between the centers of mass of the two nanoparticles is denoted as r_{com} . The vector d is defined as the distance from the center of mass of one nanoparticle pointing towards the center of the other.

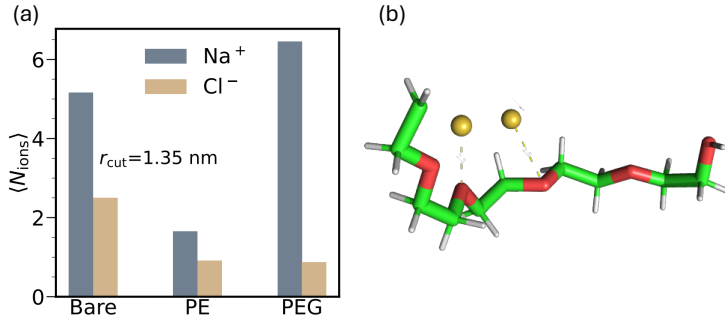


FIG. S3. Ion structuring in the cavity formed by two PE-grafted Si-NPs. (a) To further understand the propensity of salt-polymer interactions, we show the number of ions inside the spherical volume defined by radial cutoff distances of $r_{\text{cut}} = 1.35 \text{ nm}$ from the Si-NP center at $T = 300 \text{ K}$, $P = 1 \text{ bar}$, and 2 M salt concentration. At $r_{\text{cut}} = 1.35 \text{ nm}$, the number of Na^+ ions exceeds that of Cl^- , with the PEG-grafted system showing the most significant difference. (b) We show a representation of Na^+ ions in the vicinity of a single PEG chain (red: ether oxygen, green: carbon, white: hydrogen). For clarity, Si-NP, water, and Cl^- have been omitted from the image.

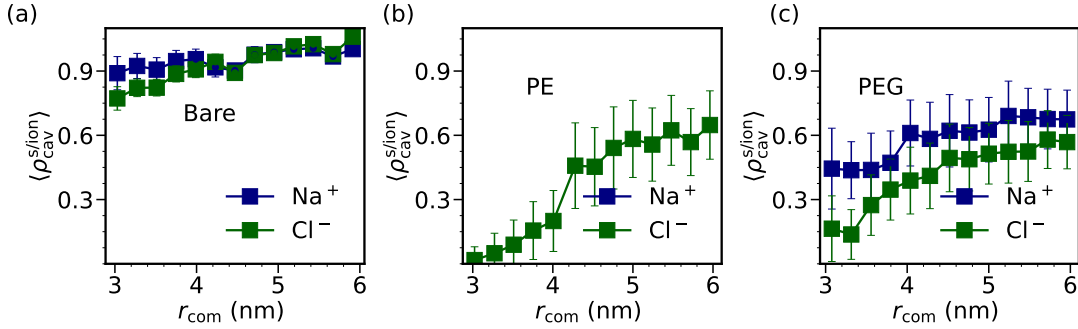


FIG. S4. Scaled ion number density in the cavity ($\langle \rho_{\text{cav}}^{\text{s/ion}} \rangle$) vs r_{com} for bare (a), PE-grafted (b), and PEG-grafted (c) Si-NPs at 1 bar and 300 K in the presence of 2 M salt concentration. The $\langle \rho_{\text{cav}}^{\text{s/ion}} \rangle$ of Cl^- decreases with decreasing r_{com} across all systems. In the PE-grafted system, both Na^+ and Cl^- exhibit a decrease in $\langle \rho_{\text{cav}}^{\text{s/ion}} \rangle$ with decreasing r_{com} , showing a sharp drop around $r_{\text{com}} = 4 \text{ nm}$, and eventually escaping the cavity near $r_{\text{com}} = 3.0 \text{ nm}$. In contrast, for hydrophilic Si-NPs (i.e., bare and PEG-grafted), Na^+ ions relatively tend to remain near the surface, indicating a relatively stronger propensity for interaction with the surface compared to Cl^- ions. These observations are aligned with recent experimental^{S1} findings, which showed that smaller monovalent cations such as Li^+ and Na^+ exhibit stronger interactions with PEG chains.

REFERENCE

[S1] M. Yu, X. Kang, and L. Qian, “Interactions between monovalent cations and polyethylene glycol: A study at micro level,” *Colloids and Surfaces A: Physicochemical and Engineering Aspects* **680**, 132731 (2024).